AMERICAN SOCIETY FOR MICROBIOLOGY | Applied and Environmental Microbiology®

ENVIRONMENTAL MICROBIOLOGY

Three-Dimensional Structure of the Ultraoligotrophic Marine Bacterium "*Candidatus* Pelagibacter ubique"

Xiaowei Zhao,[a] Cindi L. Schwartz,[b]* Jason Pierson,[b]* Stephen J. Giovannoni,[c] J. Richard McIntosh,[b] Daniela Nicastro[a,b]

Departments of Cell Biology and Biophysics, University of Texas Southwestern Medical Center, Dallas, Texas, USA[a]; Department of Molecular, Cellular, and Developmental Biology, University of Colorado, Boulder, Colorado, USA[b]; Department of Microbiology, Oregon State University, Corvallis, Oregon, USA[c]

ABSTRACT SAR11 bacteria are small, heterotrophic, marine alphaproteobacteria found throughout the oceans. They thrive at the low nutrient concentrations typical of open ocean conditions, although the adaptations required for life under those conditions are not well understood. To illuminate this issue, we used cryo-electron tomography to study "*Candidatus* Pelagibacter ubique" strain HTCC1062, a member of the SAR11 clade. Our results revealed its cellular dimensions and details of its intracellular organization. Frozen-hydrated cells, which were preserved in a life-like state, had an average cell volume (enclosed by the outer membrane) of 0.037 ± 0.011 μm^3. Strikingly, the periplasmic space occupied ~20% to 50% of the total cell volume in log-phase cells and ~50% to 70% in stationary-phase cells. The nucleoid occupied the convex side of the crescent-shaped cells and the ribosomes predominantly occupied the concave side, at a relatively high concentration of 10,000 to 12,000 ribosomes/μm^3. Outer membrane pore complexes, likely composed of PilQ, were frequently observed in both log-phase and stationary-phase cells. Long filaments, most likely type IV pili, were found on dividing cells. The physical dimensions, intracellular organization, and morphological changes throughout the life cycle of "*Ca.* Pelagibacter ubique" provide structural insights into the functional adaptions of these oligotrophic ultramicrobacteria to their habitat.

IMPORTANCE Bacterioplankton of the SAR11 clade (*Pelagibacterales*) are of interest because of their global biogeochemical significance and because they appear to have been molded by unusual evolutionary circumstances that favor simplicity and efficiency. They have adapted to an ecosystem in which nutrient concentrations are near the extreme limits at which transport systems can function adequately, and they have evolved streamlined genomes to execute only functions essential for life. However, little is known about the actual size limitations and cellular features of living oligotrophic ultramicrobacteria. In this study, we have used cryo-electron tomography to obtain accurate physical information about the cellular architecture of "*Candidatus* Pelagibacter ubique," the first cultivated member of the SAR11 clade. These results provide foundational information for answering questions about the cell architecture and functions of these ultrasmall oligotrophic bacteria.

KEYWORDS ultramicrobacteria, cryo-electron tomography, type IV pili, PilQ, SAR11

The SAR11 clade of heterotrophic marine alphaproteobacteria, which is now widely accepted as the most successful clade of organisms on Earth, includes the bacterium "*Candidatus* Pelagibacter ubique" (herein referred to as *Pelagibacter*). SAR11 members are distributed throughout the global oceans and account for about 25% of all plankton cells (1, 2). These organisms survive at levels of nutrition at which most would starve, and they are thought to play a major role in carbon cycling on Earth (3).

Received 8 October 2016 **Accepted** 9 November 2016

Accepted manuscript posted online 11 November 2016

Citation Zhao X, Schwartz CL, Pierson J, Giovannoni SJ, McIntosh JR, Nicastro D. 2017. Three-dimensional structure of the ultraoligotrophic marine bacterium "*Candidatus* Pelagibacter ubique." Appl Environ Microbiol 83:e02807-16. https://doi.org/10.1128/AEM.02807-16.

Editor Claire Vieille, Michigan State University

Address correspondence to Daniela Nicastro, daniela.nicastro@utsouthwestern.edu.

* Present address: Cindi L. Schwartz, Rocky Mountain Laboratories, NIAID, NIH, Hamilton, Montana, USA; Jason Pierson, FEI Co., Hillsboro, Oregon, USA.

They are among the smallest free-living cells known (2) and have among the smallest genomes found in autonomously replicating cells (4, 5), probably as a result of genomic streamlining (6). Nonetheless, *Pelagibacter* genomes appear to encode nearly all of the basic functions of alphaproteobacterial cells, which enables the organisms to grow in low-nutrient ocean systems. The abilities of SAR11 cells to compete for nutrients and to replicate efficiently probably explain their successful colonization of the oceans. The *Pelagibacter* strain used in this study, HTCC1062, is typical of SAR11 organisms that occupy the surface waters of temperate and polar oceans.

Oligotrophic marine bacteria occupy a special place in the literature regarding small cells because natural populations of marine bacteria, particularly those from ocean gyres where nutrients are present in extremely low abundance, often approach the theoretical limits for the smallest cells that can be imagined, based on fundamental biological considerations. The term "ultramicrobacteria" was coined to describe the size of such bacterial cells ($<$0.1 μm^3), which are abundant (0.2×10^6 to 2×10^6 cells/ml) in aquatic ecosystems (7). Theories explaining the small size of these organisms usually argue either that the organisms are small because they are starved or that small size is selectively favored in very-low-nutrient ecosystems. Accumulating data have demonstrated that bacterioplankton spend much of their time growing and are active in geochemical cycles (8), although undoubtedly such cells endure periods when nutrient limitation shuts down replication (9). The alternative explanation, i.e., that small size can make cells more competitive, assumes either that the reduced material costs of replicating drive minimization (6) or that high surface-to-volume ratios make cells more competitive for nutrients (10). For example, in some conceptual models, surface-to-volume relationships are recognized as potentially important factors influencing the balance between nutrient transport capacity and biomass (11). In one model, large cells are not competitive in dilute ecosystems because they waste energy producing metabolic enzymes that will never be pushed to process substrates at close to their turnover capacity (10). Other studies have examined the relationships between the number of periplasmic substrate binding proteins and whole-cell kinetics, yielding the conclusion that a higher ratio of substrate binding proteins to cytoplasmic proteins provides cells with kinetic properties that are favorable at very low nutrient concentrations (12). *Pelagibacterales* are the most abundant planktonic organisms in the oceans and were reported as the smallest free-living cells (0.01 μm^3) when they were first cultivated in a laboratory (2). Subsequent fluorescence microscopy measurements indicated that SAR11 bacteria from different oceanic regions were typically as large as, if not larger than, other prokaryotes (3). Modeling efforts aimed at a better understanding of the functional adaptions of oligotrophic ultramicrobacteria will benefit from accurate data on cell dimensions.

Cryo-electron tomography (cryo-ET) has been successfully used for *in situ* structural analysis of both prokaryotic and eukaryotic cells, because of its ability to reveal a life-like, frozen-hydrated state with resolution suitable for determining the macromolecular organization of intact cells (13–17). As a specimen is tilted in the electron beam, a set of two-dimensional (2D) projection images can be collected and used to reconstruct a three-dimensional (3D) image of the object, allowing 3D modeling. In addition, rapid freezing (which occurs within $\sim$1 ms) preserves the cells in a nearly native state without chemical fixation or staining, which allows accurate measurement and examination of the cell dimensions and internal structures. In the past few years, cryo-ET has yielded great insights into the internal organization of many commonly studied Gram-negative bacteria (18–20), archaebacteria (21), cyanobacteria (22), mycobacteria and mycoplasmae (23), viruses (24, 25), and bacterial phages (26) and, more recently, the cellular architecture of eukaryotes (27, 28).

In this study, we used cryo-ET to visualize the 3D structure of frozen-hydrated *Pelagibacter* cells. The cryopreserved cells were considerably larger than the glutaraldehyde-fixed specimens of the same strain that were studied previously (2). However, our images revealed very small cells with a proportionately large periplasmic space, an eccentrically located nucleoid occupying nearly one-half of the cytoplasm,

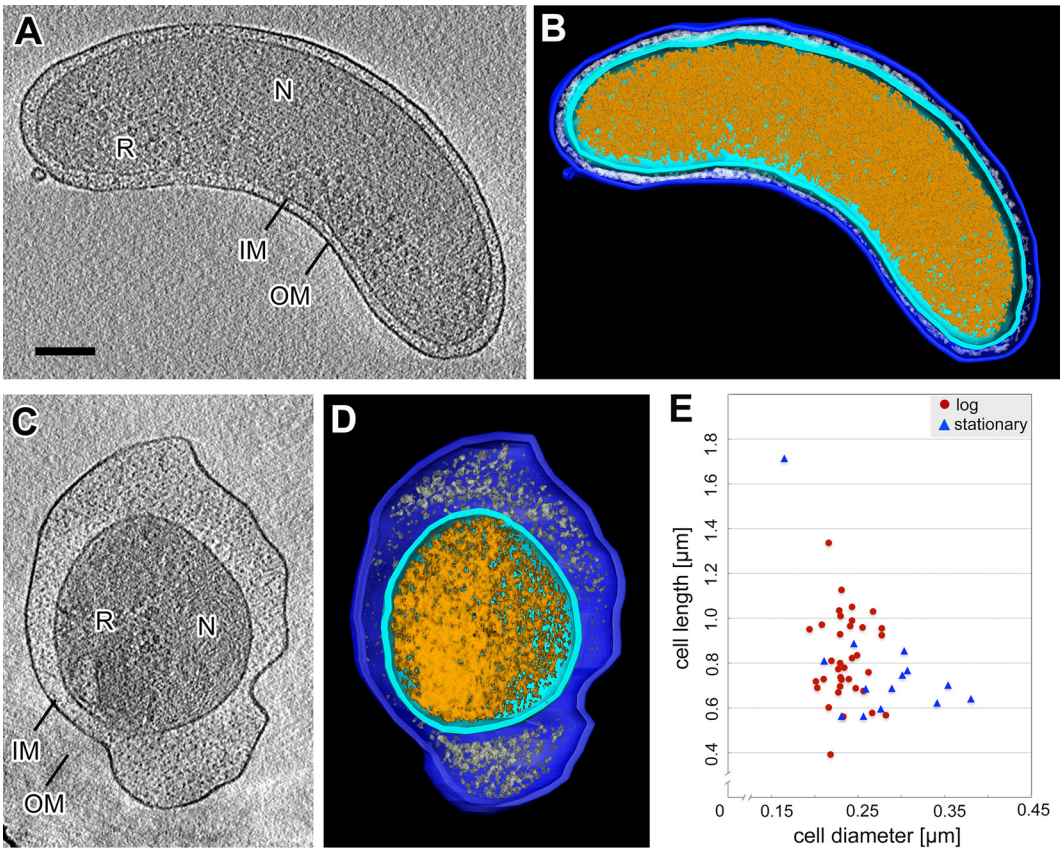

FIG 1 Cryo-electron tomography of intact frozen-hydrated *Pelagibacter* cells. (A) A 15-nm-thick tomographic slice of a *Pelagibacter* cell grown in the log phase. Note the uniform periplasmic space between the outer membrane (OM) and the inner membrane (IM). The region occupied by the nucleoid (N) shows a filamentous structure and lacks larger ribosome-like complexes (R). (B) Surface-rendered 3D model of the *Pelagibacter* cell shown in panel A. Note that the model was sliced open to allow viewing of the cell inside. Modeled structures include the OM (dark blue), IM (cyan), peptidoglycan layer (white), and cytoplasm (orange). (C) A 15-nm-thick tomographic slice of a *Pelagibacter* cell grown in the stationary phase. The cell morphology is more spherical and the periplasmic space is dramatically increased, compared to log-phase cells. (D) Surface-rendered 3D model of the *Pelagibacter* cell shown in panel C. Note that the model was sliced open to allow viewing of the cell inside. (E) Distribution of cell length and cell diameter values among all 50 reconstructed *Pelagibacter* cells. Of the studied cells, 36 were from cultures in the log phase and 14 from cultures in the stationary phase. Scale bar, 100 nm (A; also valid for panel C).

and a high ribosome concentration in relation to the *Pelagibacter* growth rate, which is less than 1 division per day. We determined the cell length distribution in late-log-phase and stationary-phase cell cultures and found hints of asymmetric cell division. In addition, we found an outer membrane (OM) pore complex that resembled PilQ secretin and cell-cycle-specific formation of extracellular filaments, most likely type IV pili.

RESULTS

Cell morphology and dimensions of *Pelagibacter*. Tomographic reconstructions of cells frozen from culture medium clearly revealed the overall morphology and subcellular organization of *Pelagibacter*. Most cells frozen at the log phase were crescent-shaped (Fig. 1A and B, 2A, and 3A to E), and only the shortest were relatively straight or oval (Fig. 3F). The lengths of cells from log-phase cultures varied from 400 to 1,300 nm (Fig. 1E). The cell diameters were less variable, however, ranging from 190 to 280 nm (among a total of 36 reconstructed cells from log-phase cultures). These data are consistent with the model that cells approximately double in length and then divide by fission (29). Cryo-ET also revealed a distinct subcellular organization in *Pelagibacter*. The cell interior appeared as two major zones, i.e., the nucleoid and a ribosome-containing area (Fig. 1A). Cells from stationary-phase cultures tended to be more

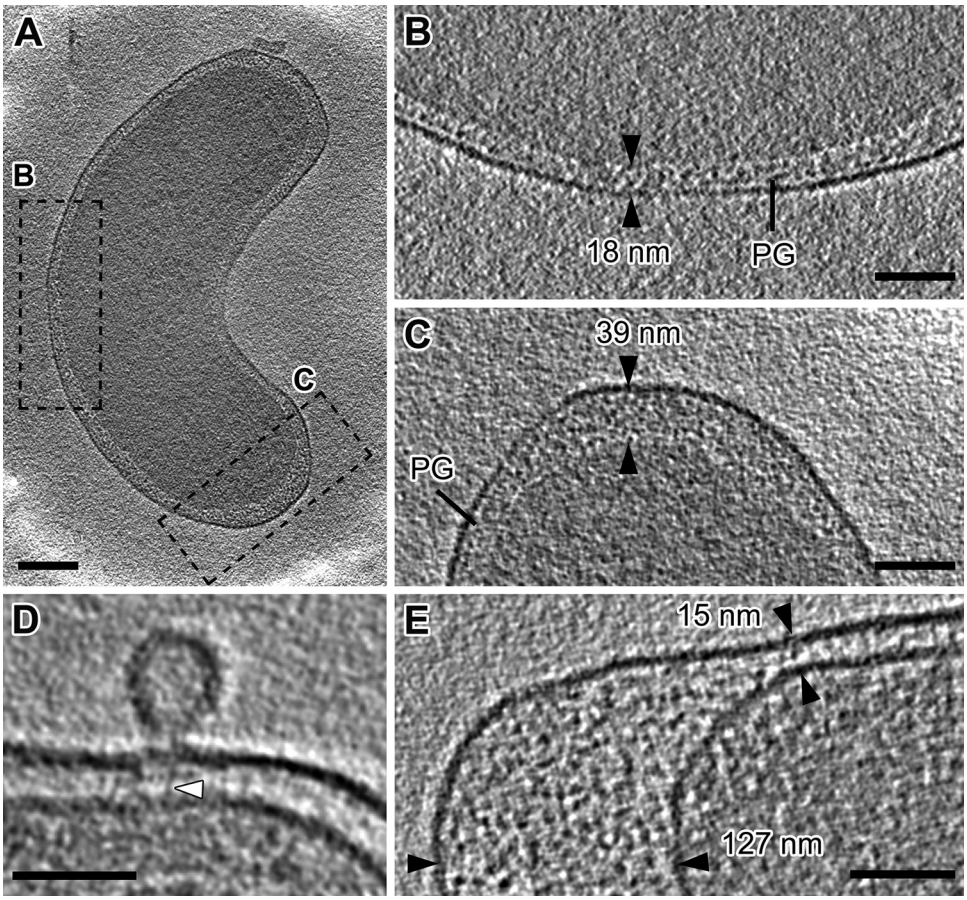

FIG 2 Characterization of the periplasmic space of *Pelagibacter*. (A) Intact *Pelagibacter* cell grown in the log phase. (B and C) Magnified images of the two periplasmic regions outlined in panel A. Along the long axis of the cells, the thickness of the periplasmic space is about 18 nm at the cell body (B). Note that two or three layers of peptidoglycan (PG) can be observed in many regions. The diameter of the periplasmic space is increased to 39 nm at the cell poles, and the PG layers become less organized (C). (D) Protuberance of the OM, resembling a vesicle. Note the tether-like structure (white arrowhead) in the periplasmic space. (E) Enlarged periplasmic space with many particles at the cell pole. The black arrowheads in panels B, C, and E indicate the measured width of the periplasmic space. Scale bars, 100 nm (A) and 50 nm (B, C, D, and E).

spherical (Fig. 1C and D), with the cell lengths ranging from 600 to 900 nm with only one very long exception (1,750 nm) (see Fig. 5E), which appeared to be a cell that failed to complete division but continued to grow. The relative volume and disposition of the subcellular compartments were different in stationary-phase cells; the cells were wider, the cytoplasm was smaller, and the volume of the periplasm was increased (Fig. 1C to E).

The membranes of these Gram-negative cells had a smooth appearance and were well preserved in our frozen-hydrated specimens (Fig. 1A to D). The reconstructed cells from log-phase cultures contained total cell volumes (enclosed by the OM) ranging from 0.015 μm^3 to 0.058 μm^3, depending on the cell length, and an average volume of 0.037 $\pm$ 0.011 μm^3 (Table 1; see also Table S1 in the supplemental material). The cell volume of *Pelagibacter* was reported previously as about 0.01 μm^3, based on measurements of negatively stained and glutaraldehyde-fixed specimens (2); the difference between our measurements and the published results was likely due to shrinkage of samples previously prepared by chemical fixation. The cell volumes of SAR11 bacteria collected from different regions of the ocean ranged between 0.031 and 0.051 μm^3 when viewed by DNA fluorescence (3), which was consistent in part with our measurements and confirmed that SAR11 cells can grow somewhat larger than thought previously.

Pronounced periplasm. The whole-cell volumes were similar for log-phase cells ($n = 30$) and stationary-phase cells ($n = 5$), but the volume of the cytoplasm was

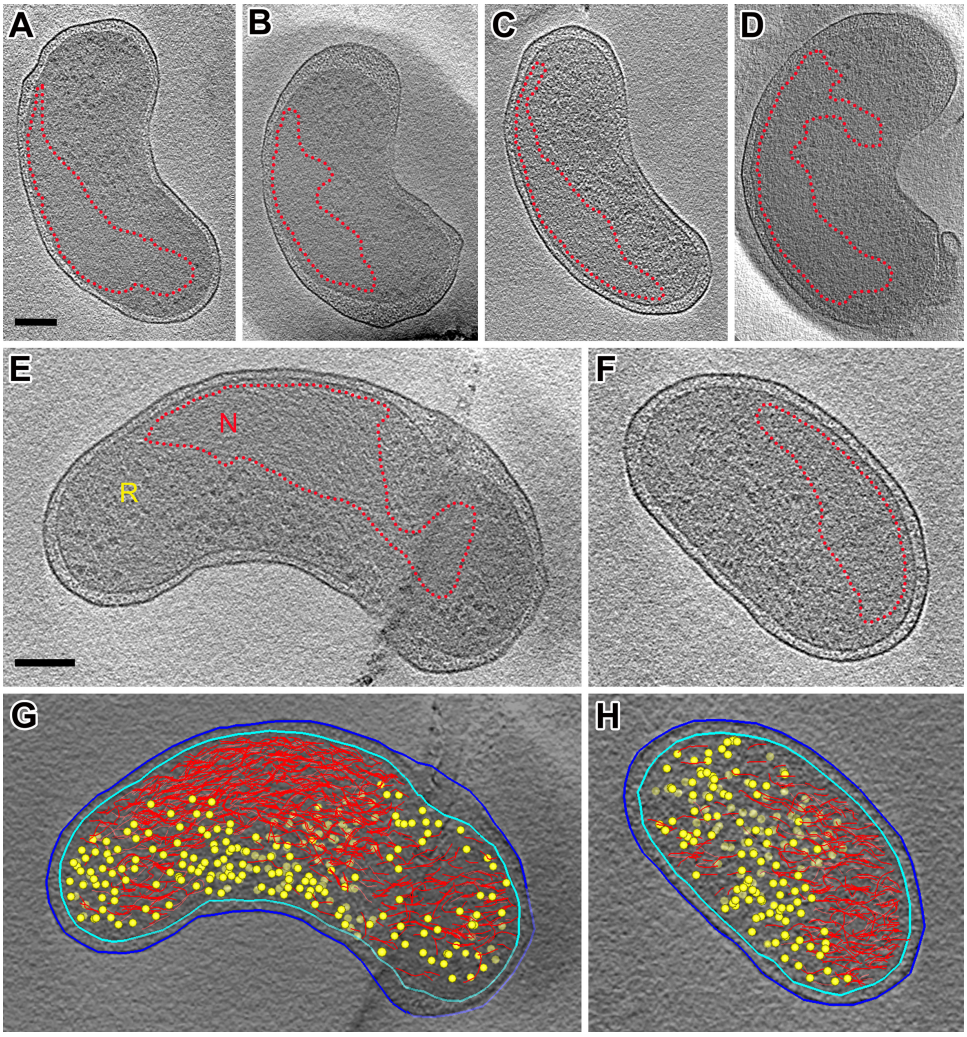

FIG 3 Characterization of the eccentrically located nucleoid, suggesting polarity along the short cell axis. (A to F) Representative *Pelagibacter* cells cultured in the log phase. The nucleoid (N) regions (outlined by red dashed lines) are always on the convex side of the cells, whereas the cytoplasm, containing ribosome-sized particles (R), is predominantly on the concave side of the cells. (G and H) 3D modeled OM (dark blue), IM (cyan), nucleoid (red), and ribosome-like particles (yellow) in the cells shown in panels E and F, respectively. Scale bars, 100 nm (A; also valid for B, C, and D) and 100 nm (E; also valid for F, G, and H).

reduced in stationary-phase cells, relative to an increased periplasmic space (Table 1). The periplasmic space of *Pelagibacter* was relatively large, occupying 20% to 50% of the total cell volume for log-phase cells and 50% to 70% for stationary-phase cells (Table 1; see also Table S1). Especially in log-phase cells, the periplasmic width was relatively uniform along the side of the cell body, with an average diameter of 17 ± 3 nm (Fig. 2A and Table S2), which was similar to that of *Escherichia coli* (30). At the cell poles, however, the periplasmic width became larger and more variable. The average periplas-

TABLE 1 Volume characteristics of log-phase and stationary-phase cells

Parameter	Log phase (30 cells)			Stationary phase (5 cells)		
	Whole-cell volume (μm^3)	Cytoplasm volume (μm^3)	Periplasm proportion (%)	Whole-cell volume (μm^3)	Cytoplasm volume (μm^3)	Periplasm proportion (%)
Minimum	0.015	0.007	21	0.026	0.011	47
Maximum	0.058	0.039	50	0.040	0.019	73
Mean	0.037	0.024	36.7	0.035	0.015	56.2
Standard deviation	0.011	0.008	7.0	0.007	0.003	10.8

mic width was 48 ± 36 nm at the poles, but the width increased to >100 nm in some cells (Fig. 2E and Table S2). Although we observed one or two layers of density in the periplasm, most likely representing peptidoglycan (Fig. 2B and C) and scattered particles (Fig. 2E), the matrix of the periplasm was more translucent than the cytoplasm, suggesting a lower density of macromolecules. Occasionally, we found small vesicles attached to the extracellular surface of the OM (Fig. 2D). Sometimes, a tether-like structure originated from the inner membrane (IM) and connected to the vesicle (white arrowhead in Fig. 2D).

Eccentrically localized nucleoid. Although the cytoplasm was considerably more crowded than the periplasm, cryo-ET revealed a distinct subcellular organization. The cell interior contained many electron-dense particles with diameters of ~20 nm; their shapes and sizes were consistent with their identification as ribosomes (Fig. 3A to F) (31). The nucleoid, which was identified by its fibrous texture and lack of ribosome-like particles, was located eccentrically at the convex side of the cell (Fig. 3A to E). Even in very short cells that displayed little curvature, presumably the products of recent cell division, the nucleoid and ribosomes were spatially segregated at opposite sides of the cell, revealing an asymmetry along one of the short cell axes (Fig. 3F). This is in contrast to the centrally located nucleoid and peripherally located ribosomes observed in many other bacterial species (18, 19, 32). Three-dimensional modeling of nucleoids and ribosome-like particles indicated that these subcellular structures were compartmentalized into two distinct zones, each taking up roughly one-half of the volume enclosed by the IM (Fig. 3G and H).

Nucleoid volume. Some bacterioplankton have evolved small genomes, making them some of the simplest free- living cells known (33, 34). One of the fundamental constraints on cell size is the physical volume occupied by the genome. Therefore, we closely examined the nucleoid of *Pelagibacter* to better understand how space is partitioned within the cytoplasm. We compared the nucleoid measurements obtained from cryo-ET (~0.012 μm^3, estimated as one-half of the cytoplasm volume) (Table 1) to the estimates of the minimal hydrated volume of the 1.3-Mb genome of *Pelagibacter* as follows. The diameter of B-DNA (with some water bound) is ~25 Å; if we treat DNA as a cylinder, then its volume (V) is $V = \pi r^2 L$, where r is 12.5 Å and the length of the DNA (L) is 3.4 Å × 1.3 × 10^6 bp (the *Pelagibacter* genome has 1.3 × 10^6 base pairs, and the distance between base pairs in the helix direction is 3.4 Å), which is equivalent to a volume of 0.0022 μm^3. This estimated DNA volume is about one-fifth of the measured nucleoid volume of *Pelagibacter*. Apparently, the packing of DNA in this organism is not tight, as would be expected for transcriptionally active DNA.

Abundance of ribosome-like particles. The fraction of the interior cell volume (surrounded by the IM) that was not occupied by the nucleoid was richly filled with electron-dense particles, which were previously interpreted as ribosomes on the basis of their size (~20 nm), shape, and contrast (31). Based on this interpretation and a template matching method (35), we detected cellular concentrations of 10,000 to 12,000 ribosome-like particles/μm^3. This observation suggests that ribosomes are relatively abundant in the *Pelagibacter* cytoplasm, considering its small volume and slow growth. The ribosome concentration of *Pelagibacter* is about twice as high as the concentration in slowly growing *E. coli* cells, although *Pelagibacter* grows significantly (30-fold) more slowly than *E. coli* (Table 2) (2, 36); however, our results are consistent with those reported in other cryo-ET studies of intact bacteria (19, 37).

Outer membrane pore complex. Pore-forming channels were found in the OM of *Pelagibacter* cells, especially in stationary-phase cells, which could be due to enhanced visibility resulting from their enlarged periplasm (Fig. 4A to C). We extracted 58 subtomogram volumes containing OM pores from the reconstructions, aligned them in three dimensions, and generated an averaged pore structure (Fig. 4D). To evaluate the subunit numbers in the pore structure, rotational symmetries ranging from 3-fold to 15-fold were applied to the subtomogram average (Fig. S1). Apparent subunit densities could be observed in most averages after the application of symmetry, but they

TABLE 2 Ribosome concentrations in various microorganisms

Organism	Growth phase	Growth rate (h^{-1})	Ribosome abundance (no./μm^3)	Cell volume (μm^3)	Reference
Escherichia coli	Rapidly growing	2.5	65,500	1.1	36
		1.5	23,900		
	Slowly growing	0.6	6,200		
Sphingomonas sp. RB2256	Mid-log	0.16	40,000	0.05–0.09	69
	Starvation	0	4,000		
Campylobacter jejuni	Mid-log	0.05	25,000[a]	0.2	19
Rickettsia prowazekii	Mid-log	0.07	17,000	0.09	68
Spiroplasma melliferum	Mid-log	>0.1	15,000[a]	0.05–0.07	37
"*Candidatus* Pelagibacter ubique"	Mid-log	0.02	10,000–12,000[a]	0.015–0.058	This study
ARMAN	Uncultivated		3,000[a]	0.03	21
WWE30OP11-OD1	Uncultivated		4,700[a]	0.009	53

[a]Ribosome abundance was estimated using cryo-ET of cells.

appeared especially strong in maps with multiples of C_3 and C_6 symmetry (Fig. S1). We further performed a rotational correlation analysis of the averaged native pore complex map, which showed peaks at 4-fold symmetry (or multiples of 4) (Fig. S1). Our analysis is consistent with previous studies reporting 12-fold symmetry for secretin pore complexes (38–44).

The pore complex has an overall width of ~13 nm (inner pore diameter, ~5 nm) and a length (perpendicular to the membrane) of ~20 nm (Fig. 4E and F), resembling the pore structures of the type II secretion system or the nonpiliated state of the type IV pilus system (Fig. 4G and H) (42, 45). In most electron microscopy (EM) reconstructions of pore-forming, nonpiliated secretins (of the type II or type III secretion system or the type IV pilus system), an apparently closed periplasmic gate was observed (42, 45, 46). Although we could see hints of a gate density in the raw tomograms of individual pores in side view (Fig. 4C and H), our averaged cryo-ET map did not show a gate. This could be caused by a "missing wedge" artifact, because our subtomogram average was dominated by top-view particles (Fig. 4B), compared to side-view ones (Fig. 4C), making densities distributed parallel to the ice layer less visible. The genome of *Pelagibacter* contains genes for PilC, PilD, PilE, PilF, and PilQ of the type II secretion system and for type IV pilus biogenesis (4). Given our structural data and information from the *Pelagibacter* genome (4), the OM pore complex could be an oligomer of PilQ secretin.

Dividing cells and pili. In our study, we also observed some dividing *Pelagibacter* cells. In one case, the cell had nearly completed the division but a small pinched-off area was still connecting the future daughter cells (Fig. 5A and B). From the different sizes of the two cells, we conclude that *Pelagibacter* organisms can undergo asymmetric cell division. Although the amount of information is too small to be statistically significant, asymmetric cell division is not uncommon among alphaproteobacteria (47). In two other cases, the cells appeared to have been frozen during the act of division (Fig. 5C to G), as suggested by constriction of the membrane (blue arrowhead in Fig. 5C). Interestingly, filaments ~3 nm in diameter and up to ~1 μm in length (Fig. 5D and E) were observed in those cells. The filaments extended predominantly from the cell division site into the extracellular space (Fig. 5C to G; see also Movie S1 in the supplemental material). Although their basal structures were not well resolved (Fig. 5D), the filaments seemed to originate from within the periplasmic space or from the IM. Based on the genomic sequence of *Pelagibacter*, which encodes the genes for type IV pilus biogenesis, including pilin PilA, OM pore PilQ, and ATPase PilT, we interpret these long filaments as type IV pili.

DISCUSSION

Very small cells have an almost irresistible philosophical allure because they embody all of the cellular features essential for life in what must approximate a minimal package. Various reviews and workshops have considered a theoretical lower limit for the size of autonomous cells from a physical and biochemical perspective, taking into

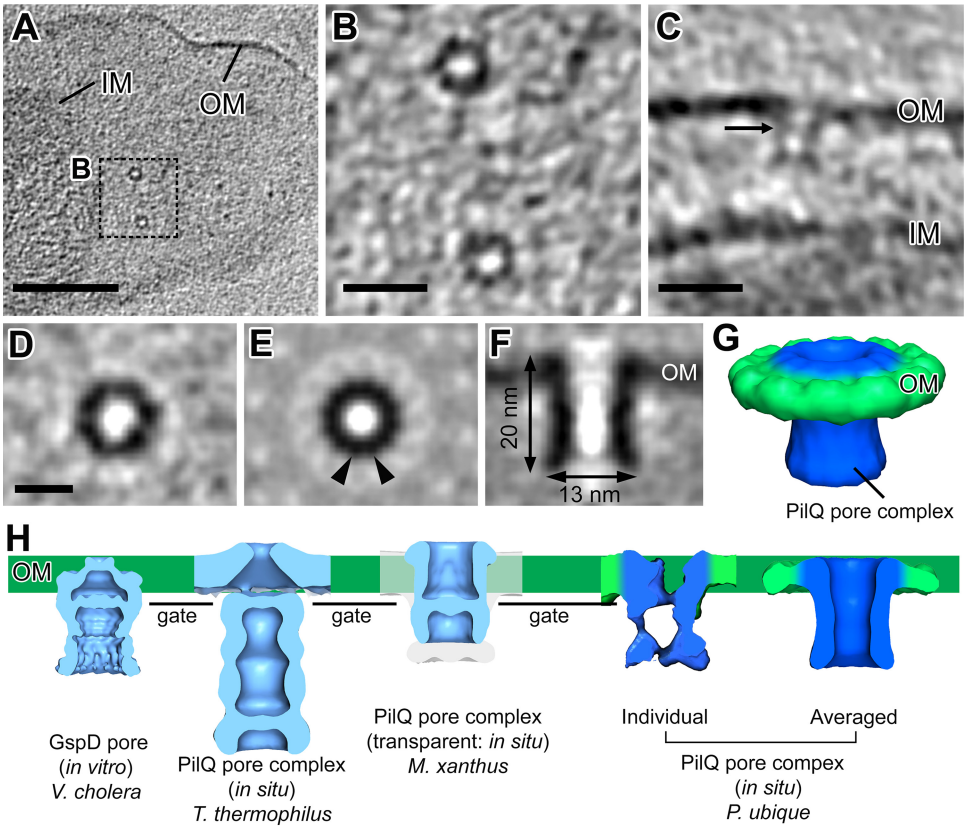

FIG 4 Outer membrane pore complexes in *Pelagibacter*. (A) Tomographic slice of a *Pelagibacter* cell in the stationary phase. Note the two pore complexes in cross-sectional view (outlined by the dashed line) in the extended periplasmic space between the outer membrane (OM) and the inner membrane (IM). (B) Magnification of the pore complexes outlined in panel A. (C) Tomographic slice of a representative *Pelagibacter* cell with the pore complex shown in side view with possible gate density (arrow). (D) Slice of a subtomogram average of 58 OM pore complexes, showing the pore in cross-sectional view. (E) Detection of subunits of the pore complex (arrowheads) after application of 12-fold symmetry to the averaged pore structure shown in panel D. (F) Side view of the 12-fold-symmetrized pore complex. (G) Surface rendering of the averaged and symmetrized pore complex (blue) embedded in the outer membrane (green). (H) Comparison of secretin pore complexes. (Left to right) *In vitro* reconstituted GspD secretin pore from *Vibrio cholerae* (Electron Microscopy Data Bank accession no. EMD-1763), native *in situ* PilQ complexes in *Thermus thermophilus* (Electron Microscopy Data Bank accession no. EMD-3022) and *Myxococcus xanthus* (the secretin domain is highlighted in blue in the transparent *in situ* map), and an individual putative PilQ pore complex (same pore as in panel C) and the averaged and 12-fold-symmetrized PilQ pore complex from "*Candidatus* Pelagibacter ubique." Scale bars, 100 nm (A), 20 nm (B and C), and 10 nm (D; also valid for E and F). The maps of *M. xanthus* PilQ are reproduced with permission (Grant Jensen, California Institute of Technology).

account the lists of essential macromolecular components and their sizes, as deduced from comparative genomics (48, 49). On the basis of those studies, a minimal viable cell diameter of ~250 nm (assuming a spherical cell) and a volume of 0.008 to 0.014 μm^3 are thought to be required for life (48). The definition of free-living is important, because some *Mycoplasma* cells are smaller (~0.013 μm^3) (50) but their genomes encode far fewer proteins. Such cells lack cell walls and outer membranes, and they can replicate only in complex media, by importing many small molecules that they cannot synthesize (51). Thus, *Mycoplasma* organisms in nature are autonomously replicating but not free-living; they are always found in direct association with eukaryotic cells. In contrast, cells of the SAR11 clade grow freely suspended throughout the marine water column.

Our cryo-ET measurements determined the authentic size of *Pelagibacter* cells as 0.015 to 0.058 μm^3, which is larger than some recently reported ultrasmall organisms; for example, marine actinobacteria have an average cell volume of ~0.013 μm^3, as analyzed by flow cytometry and microscopic fluorescence *in situ* hybridization (FISH) (52). Cells of a novel archaeon, namely, Archaeal Richmond Mine acidophilic nanoor-

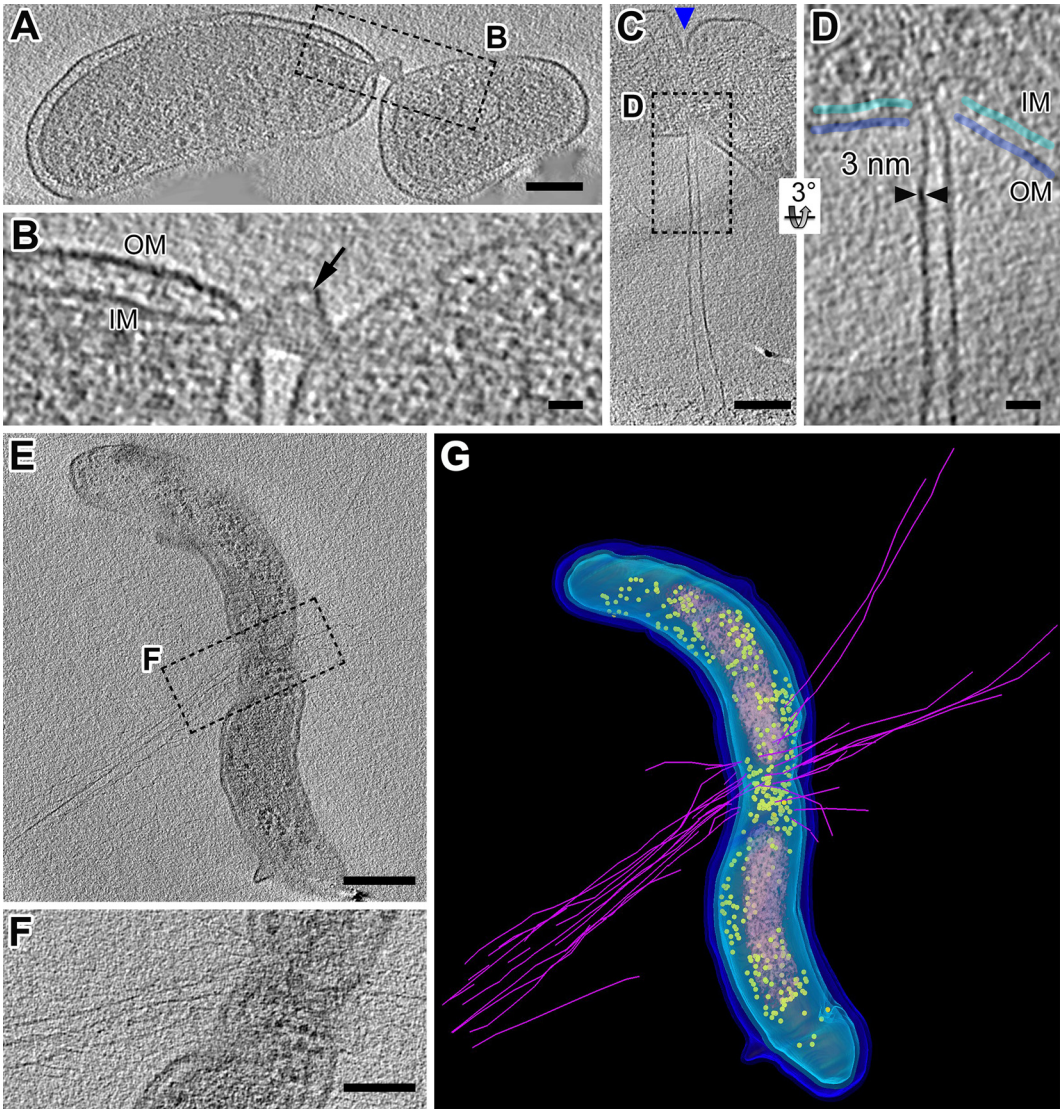

FIG 5 Dividing *Pelagibacter* cells and pili. (A) Tomographic slice showing asymmetric cell division. (B) Magnification of the region outlined in panel A. Note the still-present intercellular connection (arrow). (C) Tomographic slice of a dividing cell with two type IV pili that attached to the carbon support film. The blue arrowhead indicates constriction of the membrane. (D) Magnification of the region outlined in panel C. The inner membrane (IM) (cyan) and outer membrane (OM) (dark blue) are indicated by transparent lines. The pili appear to originate from the IM. The black arrowheads indicate the measured pilus diameter. (E) Tomographic slice of a dividing cell with many pili originating from the dividing site. (F) Magnification of the division site with pili that was outlined in panel E. (G) 3D model of the dividing cell shown in panel E. The pili (magenta), OM (dark blue), IM (cyan), nucleoid (pink), and ribosome-like particles (yellow) are shown. Scale bars, 100 nm (A, C, and F), 20 nm (B and D), and 200 nm (E).

ganisms (ARMAN), have volumes of 0.009 to 0.04 μm^3, as determined by cryo-ET (21). More recently, diverse uncultivated ultrasmall bacterial cells were found in groundwater; those cells consistently had small sizes of 0.004 to 0.013 μm^3, as shown by cryo-ET, despite some morphological variations (53). However, since the genomes of those ultrasmall groundwater bacteria were smaller than the genomes typical of free-living cells, it was suggested that those organisms were at least partially dependent on other community members for basic metabolic building blocks.

By combining a small volume with a crescent shape, *Pelagibacter* achieves an even higher surface-to-volume ratio than would otherwise be possible. The mechanism for maintaining a clearly defined shape in bacteria is thought to depend on a bacterial cytoskeleton (54–57). In *Caulobacter crescentus*, two cytoskeletal proteins, MreB and CreS (crescentin), which are actin and intermediate filament (IF) homologues, respec-

tively, are responsible for the characteristic crescent shape (58–60). MreB is required to determine a rod shape, and CreS is thought to induce cell curvature. The cytoskeleton biogenesis genes *mreB*, *mreC*, and *mreD* are found in the *Pelagibacter* genome. CreS is unique to *Caulobacter* and does not have homologues in other bacteria. However, bacterial IF-like proteins, including CreS, share a coiled-coil rod domain as a key structural feature. Genome comparisons among 26 arbitrarily selected bacteria, including *Pelagibacter*, identified at least one IF-like protein (based on the putative coiled-coil rod domain) encoded in the genomes of the overwhelming majority of the bacteria (61). The *Pelagibacter* genome encodes two uncharacterized proteins with putative coiled-coil rod domains, suggesting that *Pelagibacter* may use IF-like proteins to maintain its crescent shape. It should be noted that, to date, the expression of these genes in *Pelagibacter* has not been studied. Among the tomograms of *Pelagibacter* cells, we have seen little evidence of filamentous cytoskeleton structures; however, this does not rule out the possibility that cytoskeletal filaments exist in *Pelagibacter*, because recent cryo-ET characterizations of cytoskeletons in many bacteria indicated that no long filamentous structures representing MreB or CreS assemblies could be identified by cryo-ET (57, 62, 63). MreB and CreS perhaps are highly dynamic or exist in cells only as short segments, which are not recognizable in cellular cryotomograms.

An unusually large fraction of the *Pelagibacter* total cell volume is periplasmic space with many particles in addition to the peptidoglycan layer, suggesting that these cells may devote large proportions of their resources to enzymes that modify and transport nutrients, such as ABC transporters involved in the transport of organic molecules (64). Another striking feature of *Pelagibacter* is that the nucleoid and the ribosome-containing volume are consistently partitioned to the convex and concave sides of cells, respectively (Fig. 3). Cell polarity, i.e., nonuniform spatial organization of subcellular components along an axis, is common for prokaryotes (65), but asymmetry along the short cell axis of bacterial cells has not been reported previously. It is unclear whether cytoskeletal elements or other physical constraints are responsible for the polar segregation of the cellular components in *Pelagibacter* (66). With the nucleoid being located against the inner cell membrane on one side, however, the interface between the nucleoid and the ribosome-containing volume that would allow cotranscriptional translation is significantly reduced. In this way, *Pelagibacter* might be less efficient in protein synthesis than other bacteria. To reduce the biomass invested in protein synthesis and to reduce the energetic expense of protein synthesis, the translation rate of ribosomes is often 3- to 4-fold lower in slowly growing bacteria than in rapidly growing bacteria (67). SAR11 bacteria were thought to be small and to have few ribosomes, but we found an abundance of ribosome-like particles, relative to the slow growth of this cell type. In Table 2, we list ribosome concentrations in several organisms, although it is not clear how comparable the estimates of ribosome concentrations determined with different methods, such as biochemical analyses and cryo-ET, are (19, 21, 36, 37, 53, 68, 69). An apparent excess of ribosomes or ribosome-like particles was found in some other slowly growing organisms, such as in *Rickettsia prowazekii* (68), *Sphingomonas* sp. RB2256 (69), *Spiroplasma melliferum* (37), and *Campylobacter jejuni* (19).

Secretins are integral membrane proteins that function as OM portals for several bacterial export pathways, including the type II and III secretin systems, type IV pilus biogenesis, and filamentous phage release (70, 71). Despite the diversity of these secretory systems, secretins have markedly similar overall structures and organizations. Secretins consist of several modular N-terminal domains that reside in the periplasm and a conserved C-terminal domain that inserts in the OM, where it forms an oligomeric, ring-shaped conduit for pilus or protein extrusion (72, 73). The pore complex seen in *Pelagibacter* has a structure similar to that of secretin GspD in the type II secretion system and to the nonpiliated PilQ secretin in the type IV pilus machinery (Fig. 4G and H) (42, 45). We also compared the sequence of *Pelagibacter* PilQ predicted from the DNA sequence with those of two other secretins, i.e., *Escherichia coli* type II secretion system GspD and *Neisseria meningitidis* PilQ, for which crystal structures have

been resolved (see Fig. S2 in the supplemental material) (73, 74). Sequence alignment indicated that *Pelagibacter* PilQ has a conserved secretin domain at its C terminus and two modular N-terminal domains (N0 and N1), suggesting that PilQ is the secretin that *Pelagibacter* uses to assemble type IV pili or other translocators across the OM. We did observe pili in *Pelagibacter* cells but in only 2 dividing cells among the 50 reconstructed cells. PilQ pore complexes, which are required for pilus biogenesis, were found in many of our reconstructed *Pelagibacter* cells, however, suggesting that most PilQ pore complexes are not involved in pilus assembly under standard growth conditions (46, 75). We speculate that these idle secretins, in their nonpiliated state, may form a second class of transporters, which may be active in DNA uptake or protein secretion (46, 76).

Type IV pili have been associated with a variety of cell processes, including twitching motility, adhesion to surfaces, aggregation, intercellular communication, transformation competence, DNA uptake, and biofilm formation (77, 78). Pili were observed previously, by scanning EM, in *Pelagibacter* cells during starvation in darkness. Greater expression of the pilin gene (*pilA*) was detected under similar conditions (79). However, the role of pili in starved *Pelagibacter* cells is not known. Adhesion to surfaces and twitching motility have not yet been observed in SAR11 cells in culture or in nature, and efforts to demonstrate DNA uptake or the use of DNA as a growth substrate by *Pelagibacter* cells have thus far been unsuccessful. However, the presence of DNA uptake and competence genes (*pilC*, *pilD*, *pilE*, *pilF*, *pilG*, *pilQ*, *comL*, and *cinA*) in the *Pelagibacter* genome suggests that this organism has the ability to acquire foreign DNA (4). Multilocus sequence typing recently showed that recombination is frequent in native SAR11 populations, indicating that these type IV pili might play an important role in the acquisition of DNA from sources outside the cells (80). Interestingly, here we found that the pili were associated with the constriction sites of dividing cells instead of the cell poles, as shown for cells with twitching motility (45); this suggests that *Pelagibacter* pili may not be involved in cell motility but may play a role during cell division. For example, *Pelagibacter* cells may use pili to attach to substrates in the ocean (such as plankton or detritus), either to assist with completion of cell fission or to allow daughter cells to float away after division, to ensure low local concentrations of cells competing for the same resources.

The SAR11 clade indisputably plays an important role in ocean ecology. *Pelagibacter*, as a cultivatable representative of this clade, is a good model organism to elucidate structure-function relationships in oligotrophic ultramicrobacteria. The results we reported here constrain the range of surface-to-volume ratios for living SAR11 cells. We also identified a large periplasmic space, an eccentrically compartmentalized nucleoid, and an abundance of ribosome-like particles, all of which provide fundamental insights into the ultraoligotrophic life cycle of SAR11 bacteria. Moreover, the *Pelagibacter* OM structures that we interpret as secretin PilQ and type IV pili may play roles in the high rates of recombination that have been observed in natural SAR11 populations (80) or may have unknown roles in substrate uptake.

MATERIALS AND METHODS

Cell cultivation. As described by Rappé et al. (2), "*Candidatus* Pelagibacter ubique" strain HTCC1062, was originally collected off the Oregon coast and cultured in the Giovannoni laboratory. This strain belongs to the Ia.1 ecotype of SAR11. Live cultures are available from the Oregon State University High Throughput Microbial Cultivation Laboratory, and the strains have been deposited in the Bigelow Laboratory for Ocean Sciences culture collection. The *Pelagibacter* cells used in this study were cultivated in autoclaved seawater on low-nutrient heterotrophic medium (LNHM) (2). Cool white light of 24 μmol photons/m^2/s was supplied in a 14-h light/10-h dark cycle. Stationary-phase cells were taken from cultures after ~4 days in the stationary phase.

Cryo-ET. Quantifoil grids with holey carbon film (copper R2/2; Quantifoil Micro Tools GmbH, Jena, Germany) were negatively glow discharged. Three-microliter volumes of bacterial cell cultures that were grown to the late log phase or the stationary phase were added to the grid, and then the cells were mixed with 1 μl of a 10-fold-concentrated solution of 10-nm colloidal gold (Sigma-Aldrich). Excess fluid was blotted from the grid with Whatman filter paper for ~2 s before the grids underwent plunge-freezing in liquid ethane using a homemade plunge freezer. Frozen-hydrated samples were imaged using a Tecnai F30 transmission electron microscope (FEI, Hillsboro, OR) under low-dose conditions. Cultures of *Pelagibacter* grow only to low cell density in the laboratory (81). Therefore, we recorded low-

and medium-magnification maps of the entire EM grid and selected grid squares, respectively. This allowed us to search the grid systematically, locate the rare cells that were embedded in vitreous ice, and then record the tilt series for the targeted cells, with a tilt range of about ±70°, angular increment of 1° to 3°, and total dose of about 100 e/Å^2. The acquisition of overview maps and tilt series was accomplished using SerialEM software (82). To increase image contrast, specimens were imaged with −6- to −10-μm defocus, using a postcolumn Gatan imaging filter (Gatan, Pleasanton, CA) in zero-loss mode, with a slit width of 20 eV. The images were recorded with a Gatan charge-coupled device (CCD) camera (2,000 by 2,000 pixels) with 9.46-Å pixel size.

Image processing, analysis, and 3D modeling. The IMOD software package was used for alignment of the tilt series images, using the 10-nm gold particles as fiducial markers, before tomograms were reconstructed by weighted back-projection (83). In Fig. 5A, two large gold fiducial clusters were manually outlined and erased during the CCD Eraser step in IMOD, to avoid ray artifacts. Subtomogram averaging was performed using PEET software (84) to average the putative PilQ pore complexes in *Pelagibacter* cells. The UCSF Chimera software package was used for 3D visualization of PilQ pore complexes by isosurface rendering (85). Cell modeling was accomplished with Amira 3D software (FEI). Ribosome-like particles were identified by size (~20 nm in diameter) within the tomograms, using cross-correlation with a globular template.

Accession number(s). Four representative cell tomograms that are reported in this study were deposited in the Electron Microscopy Data Bank, with accession numbers EMD-8326 (a log-phase cell), EMD-8327 (a stationary-phase cell), EMD-8328 (a dividing cell with pili), and EMD-8329 (dividing and almost separated cells). The averaged map of the native PilQ pore complex of *Pelagibacter* was deposited under accession number EMD-8330.

SUPPLEMENTAL MATERIAL

Supplemental material for this article may be found at https://doi.org/10.1128/AEM.02807-16.

TEXT S1, PDF file, 2.3 MB.
MOVIE S1, AVI file, 18.6 MB.

ACKNOWLEDGMENTS

We are grateful to H. J. Tripp and J. C. Cho for providing the *Pelagibacter* cultures, to Pu Shing Ho for calculating the B-DNA volume, and to Y. W. Chang, Davi Ortega, and G. Jensen for generously providing the PilQ map of *M. xanthus* and discussing PilQ. We also thank Xiangan Liu for the rotational correlation analysis of the *Pelagibacter* PilQ density.

This work was supported by an NIH grant to J.R.M. (grant RR00592) and a Marine Microbiology Initiative Investigator Grant from the Gordon and Betty Moore Foundation (grant GBMF607.01). The funders had no role in study design, data collection and interpretation, or the decision to submit the work for publication.

REFERENCES

1. Morris RM, Rappé MS, Connon SA, Vergin KL, Siebold WA, Carlson CA, Giovannoni SJ. 2002. SAR11 clade dominates ocean surface bacterioplankton communities. Nature 420:806–810. https://doi.org/10.1038/nature01240.
2. Rappé MS, Connon SA, Vergin KL, Giovannoni SJ. 2002. Cultivation of the ubiquitous SAR11 marine bacterioplankton clade. Nature 418:630–633. https://doi.org/10.1038/nature00917.
3. Malmstrom RR, Kiene RP, Cottrell MT, Kirchman DL. 2004. Contribution of SAR11 bacteria to dissolved dimethylsulfoniopropionate and amino acid uptake in the North Atlantic Ocean. Appl Environ Microbiol 70:4129–4135. https://doi.org/10.1128/AEM.70.7.4129-4135.2004.
4. Giovannoni SJ, Tripp HJ, Givan S, Podar M, Vergin KL, Baptista D, Bibbs L, Eads J, Richardson TH, Noordewier M, Rappé MS, Short JM, Carrington JC, Mathur EJ. 2005. Genome streamlining in a cosmopolitan oceanic bacterium. Science 309:1242–1245. https://doi.org/10.1126/science.1114057.
5. Grote J, Thrash JC, Huggett MJ, Landry ZC, Carini P, Giovannoni SJ, Rappé MS. 2012. Streamlining and core genome conservation among highly divergent members of the SAR11 clade. mBio 3:e00252-12. https://doi.org/10.1128/mBio.00252-12.
6. Giovannoni SJ, Cameron Thrash J, Temperton B. 2014. Implications of streamlining theory for microbial ecology. ISME J 8:1553–1565. https://doi.org/10.1038/ismej.2014.60.
7. Cavicchioli R, Ostrowski M, Fegatella F, Goodchild A, Guixa-Boixereu N. 2003. Life under nutrient limitation in oligotrophic marine environments: an eco/physiological perspective of *Sphingopyxis alaskensis* (formerly *Sphingomonas alaskensis*). Microb Ecol 45:203–217. https://doi.org/10.1016/S0168-6496(03)00157-0.
8. Kirchman DL. 2016. Growth rates of microbes in the oceans. Annu Rev Mar Sci 8:285–309. https://doi.org/10.1146/annurev-marine-122414-033938.
9. Pomeroy LR. 1974. The ocean's food web, a changing paradigm. Bioscience 24:499–504. https://doi.org/10.2307/1296885.
10. Button DK. 1991. Biochemical basis for whole-cell uptake kinetics: specific affinity, oligotrophic capacity, and the meaning of the Michaelis constant. Appl Environ Microbiol 57:2033–2038.
11. Button DK, Robertson B, Gustafson E, Zhao X. 2004. Experimental and theoretical bases of specific affinity, a cytoarchitecture-based formulation of nutrient collection proposed to supercede the Michaelis-Menten paradigm of microbial kinetics. Appl Environ Microbiol 70:5511–5521. https://doi.org/10.1128/AEM.70.9.5511-5521.2004.
12. Bosdriesz E, Magnusdottir S, Bruggeman FJ, Teusink B, Molenaar D. 2015. Binding proteins enhance specific uptake rate by increasing the substrate-transporter encounter rate. FEBS J 282:2394–2407. https://doi.org/10.1111/febs.13289.
13. Engel BD, Schaffer M, Kuhn Cuellar L, Villa E, Plitzko JM, Baumeister W. 2015. Native architecture of the *Chlamydomonas* chloroplast revealed by in situ cryo-electron tomography. Elife 4:e04889. https://doi.org/10.7554/eLife.04889.
14. Baumeister W. 2002. Electron tomography: towards visualizing the mo-

lecular organization of the cytoplasm. Curr Opin Struct Biol 12:679–684. https://doi.org/10.1016/S0959-440X(02)00378-0.
15. McIntosh R, Nicastro D, Mastronarde D. 2005. New views of cells in 3D: an introduction to electron tomography. Trends Cell Biol 15:43–51. https://doi.org/10.1016/j.tcb.2004.11.009.
16. Milne JL, Subramaniam S. 2009. Cryo-electron tomography of bacteria: progress, challenges and future prospects. Nat Rev Microbiol 7:666–675. https://doi.org/10.1038/nrmicro2183.
17. Asano S, Engel BD, Baumeister W. 2016. In situ cryo-electron tomography: a post-reductionist approach to structural biology. J Mol Biol 428:332–343. https://doi.org/10.1016/j.jmb.2015.09.030.
18. Borgnia MJ, Subramaniam S, Milne JL. 2008. Three-dimensional imaging of the highly bent architecture of *Bdellovibrio bacteriovorus* by using cryo-electron tomography. J Bacteriol 190:2588–2596. https://doi.org/10.1128/JB.01538-07.
19. Muller A, Beeby M, McDowall AW, Chow J, Jensen GJ, Clemons WM, Jr. 2014. Ultrastructure and complex polar architecture of the human pathogen *Campylobacter jejuni*. Microbiologyopen 3:702–710. https://doi.org/10.1002/mbo3.200.
20. Lin T, Gao L, Zhao X, Liu J, Norris SJ. 2015. Mutations in the *Borrelia burgdorferi* flagellar type III secretion system genes *fliH* and *flil* profoundly affect spirochete flagellar assembly, morphology, motility, structure, and cell division. mBio 6:e00579-15. https://doi.org/10.1128/mBio.00579-15.
21. Comolli LR, Baker BJ, Downing KH, Siegerist CE, Banfield JF. 2009. Three-dimensional analysis of the structure and ecology of a novel, ultra-small archaeon. ISME J 3:159–167. https://doi.org/10.1038/ismej.2008.99.
22. Ting CS, Hsieh C, Sundararaman S, Mannella C, Marko M. 2007. Cryo-electron tomography reveals the comparative three-dimensional architecture of *Prochlorococcus*, a globally important marine cyanobacterium. J Bacteriol 189:4485–4493. https://doi.org/10.1128/JB.01948-06.
23. Henderson GP, Jensen GJ. 2006. Three-dimensional structure of *Mycoplasma pneumoniae*'s attachment organelle and a model for its role in gliding motility. Mol Microbiol 60:376–385. https://doi.org/10.1111/j.1365-2958.2006.05113.x.
24. Dai W, Fu C, Raytcheva D, Flanagan J, Khant HA, Liu X, Rochat RH, Haase-Pettingell C, Piret J, Ludtke SJ, Nagayama K, Schmid MF, King JA, Chiu W. 2013. Visualizing virus assembly intermediates inside marine cyanobacteria. Nature 502:707–710. https://doi.org/10.1038/nature12604.
25. Schur FK, Hagen WJ, Rumlova M, Ruml T, Muller B, Krausslich HG, Briggs JA. 2015. Structure of the immature HIV-1 capsid in intact virus particles at 8.8 Å resolution. Nature 517:505–508. https://doi.org/10.1038/nature13838.
26. Hu B, Margolin W, Molineux IJ, Liu J. 2015. Structural remodeling of bacteriophage T4 and host membranes during infection initiation. Proc Natl Acad Sci U S A 112:E4919–E4928. https://doi.org/10.1073/pnas.1501064112.
27. Mahamid J, Pfeffer S, Schaffer M, Villa E, Danev R, Cuellar LK, Forster F, Hyman AA, Plitzko JM, Baumeister W. 2016. Visualizing the molecular sociology at the HeLa cell nuclear periphery. Science 351:969–972. https://doi.org/10.1126/science.aad8857.
28. von Appen A, Kosinski J, Sparks L, Ori A, DiGuilio AL, Vollmer B, Mackmull MT, Banterle N, Parca L, Kastritis P, Buczak K, Mosalaganti S, Hagen W, Andres-Pons A, Lemke EA, Bork P, Antonin W, Glavy JS, Bui KH, Beck M. 2015. In situ structural analysis of the human nuclear pore complex. Nature 526:140–143. https://doi.org/10.1038/nature15381.
29. Li Z, Trimble MJ, Brun YV, Jensen GJ. 2007. The structure of FtsZ filaments in vivo suggests a force-generating role in cell division. EMBO J 26:4694–4708. https://doi.org/10.1038/sj.emboj.7601895.
30. Matias VR, Al-Amoudi A, Dubochet J, Beveridge TJ. 2003. Cryo-transmission electron microscopy of frozen-hydrated sections of *Escherichia coli* and *Pseudomonas aeruginosa*. J Bacteriol 185:6112–6118. https://doi.org/10.1128/JB.185.20.6112-6118.2003.
31. Gilbert RJ, Fucini P, Connell S, Fuller SD, Nierhaus KH, Robinson CV, Dobson CM, Stuart DI. 2004. Three-dimensional structures of translating ribosomes by cryo-EM. Mol Cell 14:57–66. https://doi.org/10.1016/S1097-2765(04)00163-7.
32. Montero Llopis P, Jackson AF, Sliusarenko O, Surovtsev I, Heinritz J, Emonet T, Jacobs-Wagner C. 2010. Spatial organization of the flow of genetic information in bacteria. Nature 466:77–81. https://doi.org/10.1038/nature09152.
33. Giovannoni SJ, Hayakawa DH, Tripp HJ, Stingl U, Givan SA, Cho JC, Oh HM, Kitner JB, Vergin KL, Rappé MS. 2008. The small genome of an abundant coastal ocean methylotroph. Environ Microbiol 10:1771–1782. https://doi.org/10.1111/j.1462-2920.2008.01598.x.
34. Rocap G, Larimer FW, Lamerdin J, Malfatti S, Chain P, Ahlgren NA, Arellano A, Coleman M, Hauser L, Hess WR, Johnson ZI, Land M, Lindell D, Post AF, Regala W, Shah M, Shaw SL, Steglich C, Sullivan MB, Ting CS, Tolonen A, Webb EA, Zinser ER, Chisholm SW. 2003. Genome divergence in two *Prochlorococcus* ecotypes reflects oceanic niche differentiation. Nature 424:1042–1047. https://doi.org/10.1038/nature01947.
35. Frangakis AS, Bohm J, Forster F, Nickell S, Nicastro D, Typke D, Hegerl R, Baumeister W. 2002. Identification of macromolecular complexes in cryoelectron tomograms of phantom cells. Proc Natl Acad Sci U S A 99:14153–14158. https://doi.org/10.1073/pnas.172520299.
36. Bremer H, Dennis PP. 2008. Modulation of chemical composition and other parameters of the cell at different exponential growth rates. EcoSal Plus https://doi.org/10.1128/ecosal.5.2.3.
37. Ortiz JO, Forster F, Kurner J, Linaroudis AA, Baumeister W. 2006. Mapping 70S ribosomes in intact cells by cryoelectron tomography and pattern recognition. J Struct Biol 156:334–341. https://doi.org/10.1016/j.jsb.2006.04.014.
38. Collins RF, Davidsen L, Derrick JP, Ford RC, Tonjum T. 2001. Analysis of the PilQ secretin from *Neisseria meningitidis* by transmission electron microscopy reveals a dodecameric quaternary structure. J Bacteriol 183:3825–3832. https://doi.org/10.1128/JB.183.13.3825-3832.2001.
39. Collins RF, Ford RC, Kitmitto A, Olsen RO, Tonjum T, Derrick JP. 2003. Three-dimensional structure of the *Neisseria meningitidis* secretin PilQ determined from negative-stain transmission electron microscopy. J Bacteriol 185:2611–2617. https://doi.org/10.1128/JB.185.8.2611-2617.2003.
40. Collins RF, Frye SA, Kitmitto A, Ford RC, Tonjum T, Derrick JP. 2004. Structure of the *Neisseria meningitidis* outer membrane PilQ secretin complex at 12 Å resolution. J Biol Chem 279:39750–39756. https://doi.org/10.1074/jbc.M405971200.
41. Chami M, Guilvout I, Gregorini M, Remigy HW, Muller SA, Valerio M, Engel A, Pugsley AP, Bayan N. 2005. Structural insights into the secretin PulD and its trypsin-resistant core. J Biol Chem 280:37732–37741. https://doi.org/10.1074/jbc.M504463200.
42. Reichow SL, Korotkov KV, Hol WG, Gonen T. 2010. Structure of the cholera toxin secretion channel in its closed state. Nat Struct Mol Biol 17:1226–1232. https://doi.org/10.1038/nsmb.1910.
43. Kowal J, Chami M, Ringler P, Muller SA, Kudryashev M, Castano-Diez D, Amstutz M, Cornelis GR, Stahlberg H, Engel A. 2013. Structure of the dodecameric *Yersinia enterocolitica* secretin YscC and its trypsin-resistant core. Structure 21:2152–2161. https://doi.org/10.1016/j.str.2013.09.012.
44. Nouwen N, Ranson N, Saibil H, Wolpensinger B, Engel A, Ghazi A, Pugsley AP. 1999. Secretin PulD: association with pilot PulS, structure, and ion-conducting channel formation. Proc Natl Acad Sci U S A 96:8173–8177. https://doi.org/10.1073/pnas.96.14.8173.
45. Chang YW, Rettberg LA, Treuner-Lange A, Iwasa J, Sogaard-Andersen L, Jensen GJ. 2016. Architecture of the type IVa pilus machine. Science 351:aad2001. https://doi.org/10.1126/science.aad2001.
46. Gold VA, Salzer R, Averhoff B, Kuhlbrandt W. 2015. Structure of a type IV pilus machinery in the open and closed state. Elife 4:e07380. https://doi.org/10.7554/eLife.07380.
47. Hallez R, Bellefontaine AF, Letesson JJ, De Bolle X. 2004. Morphological and functional asymmetry in α-proteobacteria. Trends Microbiol 12:361–365. https://doi.org/10.1016/j.tim.2004.06.002.
48. National Research Council. 1999. Size limits of very small microorganisms: proceedings of a workshop. National Academy Press, Washington, DC.
49. Duda VI, Suzina NE, Polivtseva VN, Boronin AM. 2012. Ultramicrobacteria: formation of the concept and contribution of ultramicrobacteria to biology. Mikrobiologiia 81:415–427. (In Russian.)
50. Seybert A, Herrmann R, Frangakis AS. 2006. Structural analysis of *Mycoplasma pneumoniae* by cryo-electron tomography. J Struct Biol 156:342–354. https://doi.org/10.1016/j.jsb.2006.04.010.
51. Fraser CM, Gocayne JD, White O, Adams MD, Clayton RA, Fleischmann RD, Bult CJ, Kerlavage AR, Sutton G, Kelley JM, Fritchman RD, Weidman JF, Small KV, Sandusky M, Fuhrmann J, Nguyen D, Utterback TR, Saudek DM, Phillips CA, Merrick JM, Tomb JF, Dougherty BA, Bott KF, Hu PC, Lucier TS, Peterson SN, Smith HO, Hutchison CA, III, Venter JC. 1995. The minimal gene complement of *Mycoplasma genitalium*. Science 270:397–403. https://doi.org/10.1126/science.270.5235.397.
52. Ghai R, Mizuno CM, Picazo A, Camacho A, Rodriguez-Valera F. 2013.

Metagenomics uncovers a new group of low GC and ultra-small marine Actinobacteria. Sci Rep 3:2471. https://doi.org/10.1038/srep02471.
53. Luef B, Frischkorn KR, Wrighton KC, Holman HY, Birarda G, Thomas BC, Singh A, Williams KH, Siegerist CE, Tringe SG, Downing KH, Comolli LR, Banfield JF. 2015. Diverse uncultivated ultra-small bacterial cells in groundwater. Nat Commun 6:6372. https://doi.org/10.1038/ncomms7372.
54. Cho H. 2015. The role of cytoskeletal elements in shaping bacterial cells. J Microbiol Biotechnol 25:307–316. https://doi.org/10.4014/jmb.1409.09047.
55. Margolin W. 2009. Sculpting the bacterial cell. Curr Biol 19:R812–R822. https://doi.org/10.1016/j.cub.2009.06.033.
56. Cabeen MT, Jacobs-Wagner C. 2010. The bacterial cytoskeleton. Annu Rev Genet 44:365–392. https://doi.org/10.1146/annurev-genet-102108-134845.
57. Pilhofer M, Jensen GJ. 2013. The bacterial cytoskeleton: more than twisted filaments. Curr Opin Cell Biol 25:125–133. https://doi.org/10.1016/j.ceb.2012.10.019.
58. Figge RM, Divakaruni AV, Gober JW. 2004. MreB, the cell shape-determining bacterial actin homologue, co-ordinates cell wall morphogenesis in *Caulobacter crescentus*. Mol Microbiol 51:1321–1332. https://doi.org/10.1111/j.1365-2958.2003.03936.x.
59. Ausmees N, Kuhn JR, Jacobs-Wagner C. 2003. The bacterial cytoskeleton: an intermediate filament-like function in cell shape. Cell 115:705–713. https://doi.org/10.1016/S0092-8674(03)00935-8.
60. Celler K, Koning RI, Koster AJ, van Wezel GP. 2013. Multidimensional view of the bacterial cytoskeleton. J Bacteriol 195:1627–1636. https://doi.org/10.1128/JB.02194-12.
61. Bagchi S, Tomenius H, Belova LM, Ausmees N. 2008. Intermediate filament-like proteins in bacteria and a cytoskeletal function in *Streptomyces*. Mol Microbiol 70:1037–1050. https://doi.org/10.1111/j.1365-2958.2008.06473.x.
62. Briegel A, Dias DP, Li Z, Jensen RB, Frangakis AS, Jensen GJ. 2006. Multiple large filament bundles observed in *Caulobacter crescentus* by electron cryotomography. Mol Microbiol 62:5–14. https://doi.org/10.1111/j.1365-2958.2006.05355.x.
63. Swulius MT, Chen S, Ding HJ, Li Z, Briegel A, Pilhofer M, Tocheva EI, Lybarger SR, Johnson TL, Sandkvist M, Jensen GJ. 2011. Long helical filaments are not seen encircling cells in electron cryotomograms of rod-shaped bacteria. Biochem Biophys Res Commun 407:650–655. https://doi.org/10.1016/j.bbrc.2011.03.062.
64. Sowell SM, Wilhelm LJ, Norbeck AD, Lipton MS, Nicora CD, Barofsky DF, Carlson CA, Smith RD, Giovanonni SJ. 2009. Transport functions dominate the SAR11 metaproteome at low-nutrient extremes in the Sargasso Sea. ISME J 3:93–105. https://doi.org/10.1038/ismej.2008.83.
65. Lewis PJ, Thaker SD, Errington J. 2000. Compartmentalization of transcription and translation in *Bacillus subtilis*. EMBO J 19:710–718. https://doi.org/10.1093/emboj/19.4.710.
66. Gitai Z, Dye N, Shapiro L. 2004. An actin-like gene can determine cell polarity in bacteria. Proc Natl Acad Sci U S A 101:8643–8648. https://doi.org/10.1073/pnas.0402638101.
67. Dethlefsen L, Schmidt TM. 2007. Performance of the translational apparatus varies with the ecological strategies of bacteria. J Bacteriol 189:3237–3245. https://doi.org/10.1128/JB.01686-06.
68. Pang H, Winkler HH. 1994. The concentrations of stable RNA and ribosomes in *Rickettsia prowazekii*. Mol Microbiol 12:115–120. https://doi.org/10.1111/j.1365-2958.1994.tb01000.x.
69. Fegatella F, Lim J, Kjelleberg S, Cavicchioli R. 1998. Implications of rRNA operon copy number and ribosome content in the marine oligotrophic ultramicrobacterium *Sphingomonas* sp. strain RB2256. Appl Environ Microbiol 64:4433–4438.
70. Genin S, Boucher CA. 1994. A superfamily of proteins involved in different secretion pathways in Gram-negative bacteria: modular structure and specificity of the N-terminal domain. Mol Gen Genet 243:112–118. https://doi.org/10.1007/BF00283883.
71. Korotkov KV, Gonen T, Hol WG. 2011. Secretins: dynamic channels for protein transport across membranes. Trends Biochem Sci 36:433–443. https://doi.org/10.1016/j.tibs.2011.04.002.
72. Burkhardt J, Vonck J, Averhoff B. 2011. Structure and function of PilQ, a secretin of the DNA transporter from the thermophilic bacterium *Thermus thermophilus* HB27. J Biol Chem 286:9977–9984. https://doi.org/10.1074/jbc.M110.212688.
73. Korotkov KV, Pardon E, Steyaert J, Hol WG. 2009. Crystal structure of the N-terminal domain of the secretin GspD from ETEC determined with the assistance of a nanobody. Structure 17:255–265. https://doi.org/10.1016/j.str.2008.11.011.
74. Berry JL, Phelan MM, Collins RF, Adomavicius T, Tonjum T, Frye SA, Bird L, Owens R, Ford RC, Lian LY, Derrick JP. 2012. Structure and assembly of a trans-periplasmic channel for type IV pili in *Neisseria meningitidis*. PLoS Pathog 8:e1002923. https://doi.org/10.1371/journal.ppat.1002923.
75. Salzer R, Kern T, Joos F, Averhoff B. 2014. Environmental factors affecting the expression of type IV pilus genes as well as piliation of *Thermus thermophilus*. FEMS Microbiol Lett 357:56–62. https://doi.org/10.1111/1574-6968.12506.
76. Schwarzenlander C, Haase W, Averhoff B. 2009. The role of single subunits of the DNA transport machinery of *Thermus thermophilus* HB27 in DNA binding and transport. Environ Microbiol 11:801–808. https://doi.org/10.1111/j.1462-2920.2008.01801.x.
77. Hazes B, Frost L. 2008. Towards a systems biology approach to study type II/IV secretion systems. Biochim Biophys Acta 1778:1839–1850. https://doi.org/10.1016/j.bbamem.2008.03.011.
78. Mattick JS. 2002. Type IV pili and twitching motility. Annu Rev Microbiol 56:289–314. https://doi.org/10.1146/annurev.micro.56.012302.160938.
79. Steindler L, Schwalbach MS, Smith DP, Chan F, Giovannoni SJ. 2011. Energy starved *Candidatus* Pelagibacter ubique substitutes light-mediated ATP production for endogenous carbon respiration. PLoS One 6:e19725. https://doi.org/10.1371/journal.pone.0019725.
80. Vergin KL, Tripp HJ, Wilhelm LJ, Denver DR, Rappé MS, Giovannoni SJ. 2007. High intraspecific recombination rate in a native population of *Candidatus* pelagibacter ubique (SAR11). Environ Microbiol 9:2430–2440. https://doi.org/10.1111/j.1462-2920.2007.01361.x.
81. Connon SA, Giovannoni SJ. 2002. High-throughput methods for culturing microorganisms in very-low-nutrient media yield diverse new marine isolates. Appl Environ Microbiol 68:3878–3885. https://doi.org/10.1128/AEM.68.8.3878-3885.2002.
82. Mastronarde DN. 2005. Automated electron microscope tomography using robust prediction of specimen movements. J Struct Biol 152:36–51. https://doi.org/10.1016/j.jsb.2005.07.007.
83. Kremer JR, Mastronarde DN, McIntosh JR. 1996. Computer visualization of three-dimensional image data using IMOD. J Struct Biol 116:71–76. https://doi.org/10.1006/jsbi.1996.0013.
84. Nicastro D, Schwartz C, Pierson J, Gaudette R, Porter ME, McIntosh JR. 2006. The molecular architecture of axonemes revealed by cryoelectron tomography. Science 313:944–948. https://doi.org/10.1126/science.1128618.
85. Pettersen EF, Goddard TD, Huang CC, Couch GS, Greenblatt DM, Meng EC, Ferrin TE. 2004. UCSF Chimera: a visualization system for exploratory research and analysis. J Comput Chem 25:1605–1612. https://doi.org/10.1002/jcc.20084.